



Soil moisture retrieval from time series multi-angular radar data using a dry down constraint

Liujun Zhu^{a,b,*}, Jeffrey P. Walker^a, Leung Tsang^b, Huanting Huang^b, Nan Ye^a, Christoph Rüdiger^a

^a Department of Civil Engineering, Monash University, Clayton, Vic. 3800, Australia

^b Department of Electrical Engineering and Computer Science, University of Michigan, Ann Arbor, MI 48109-2122, USA

ARTICLE INFO

Edited by: Jing M. Chen

Keywords:

Soil moisture
Multi-temporal
Multi-angular
Synthetic aperture radar

ABSTRACT

Multi-angular and multi-temporal methods have been developed and accepted as two promising strategies for reliable soil moisture retrieval from radar data. However, the way to combine time series multi-angular data acquired from both descending and ascending orbits with different imaging modes (e.g., ScanSAR and Stripmap) remains unresolved. Consequently, a multi-temporal algorithm is proposed for soil moisture retrieval at the pixel – paddock scale (25–500 m) using time series multi-angular L-band (1.26 GHz) radar data. The method assumes time-invariant roughness and vegetation for the retrieval period together with a soil moisture dry-down constraint for noise reduction, while utilizing multi-angular data without incidence angle normalization. The Numerical Maxwell Model of Three-Dimensional simulations and distorted Born approximation (NMM3D-DBA) were used to build a set of landcover specific multi-angular look up tables (LUTs). Effective isotropic roughness values were assumed suitably able to account for the periodic features in cultivated surfaces, with values determined as part of the soil moisture retrieval. A genetic algorithm was used to minimize the difference between LUTs and time series multi-angular radar observations with the dry-down constraint. Evaluation based on the Fifth Soil Moisture Active Passive Experiment dataset (SMAPEX-5) has shown an acceptable overall root mean square error (RMSE) of $0.070 \text{ m}^3/\text{m}^3$ at the 25-m pixel scale and $0.056 \text{ m}^3/\text{m}^3$ at the paddock (field) scale ($\sim 0.1\text{--}0.5 \text{ km}$). Further investigations on the effect of polarization combination and time interval of radar data have confirmed the effectiveness of the proposed method for irregularly collected data with different imaging modes.

1. Introduction

Synthetic aperture radar (SAR) has demonstrated its potential for soil moisture mapping at high spatial resolution over the past four decades (Kornelsen and Coulibaly, 2013). However, soil moisture retrieval from SAR data still faces challenges, due to the dependence of microwave signals on geophysical parameters besides soil moisture, including the soil roughness, vegetation water content (VWC) and vegetation structure (Balenzano et al., 2011; Kornelsen and Coulibaly, 2013).

A forward model that can accurately describe the effect of these geophysical parameters on SAR observations is a necessary but insufficient requirement for soil moisture retrieval. Commonly used soil surface scattering models in literature include the semi-empirical Oh model (Oh et al., 2002), Dubois model (Dubois et al., 1995), and the physically based Integral Equation Model (IEM, Fung et al., 1992) or variants (e.g., Baghdadi et al., 2016; Chen et al., 2003). These surface

scattering models are commonly integrated with vegetation scattering models, such as the semi-empirical water cloud model (WCM, Attema and Ulaby, 1978) and physically-based alternatives (e.g., Lang and Sighu, 1983; Ulaby et al., 1990) so as to predict the scattering of vegetated areas. The performance of these models is dependent on their inherent approximations and/or the accuracy of the radar-configuration-specific tuning parameters (Kornelsen and Coulibaly, 2013). Recently, the numerical solutions of Maxwell's equations in three dimension (NMM3D, Huang et al., 2017b; Huang and Tsang, 2012; Huang et al., 2010) has been used to accurately represent rough surface scattering by way of look up tables (LUTs), to overcome the computational demands in real-time soil moisture retrieval (Kim et al., 2012a, 2014). Despite the slight improvement in accuracy (up to 2 dB) compared with the advanced IEM (Huang et al., 2010), such an approach is currently hampered by the limited availability of LUTs.

Additional limitations are in the inversion of these models or LUTs, due to the ill-posed nature of the problem, caused by the large number

* Corresponding author at: Department of Civil Engineering, Monash University, Clayton, Vic. 3800, Australia.

E-mail address: Liujun.Zhu@monash.edu (L. Zhu).

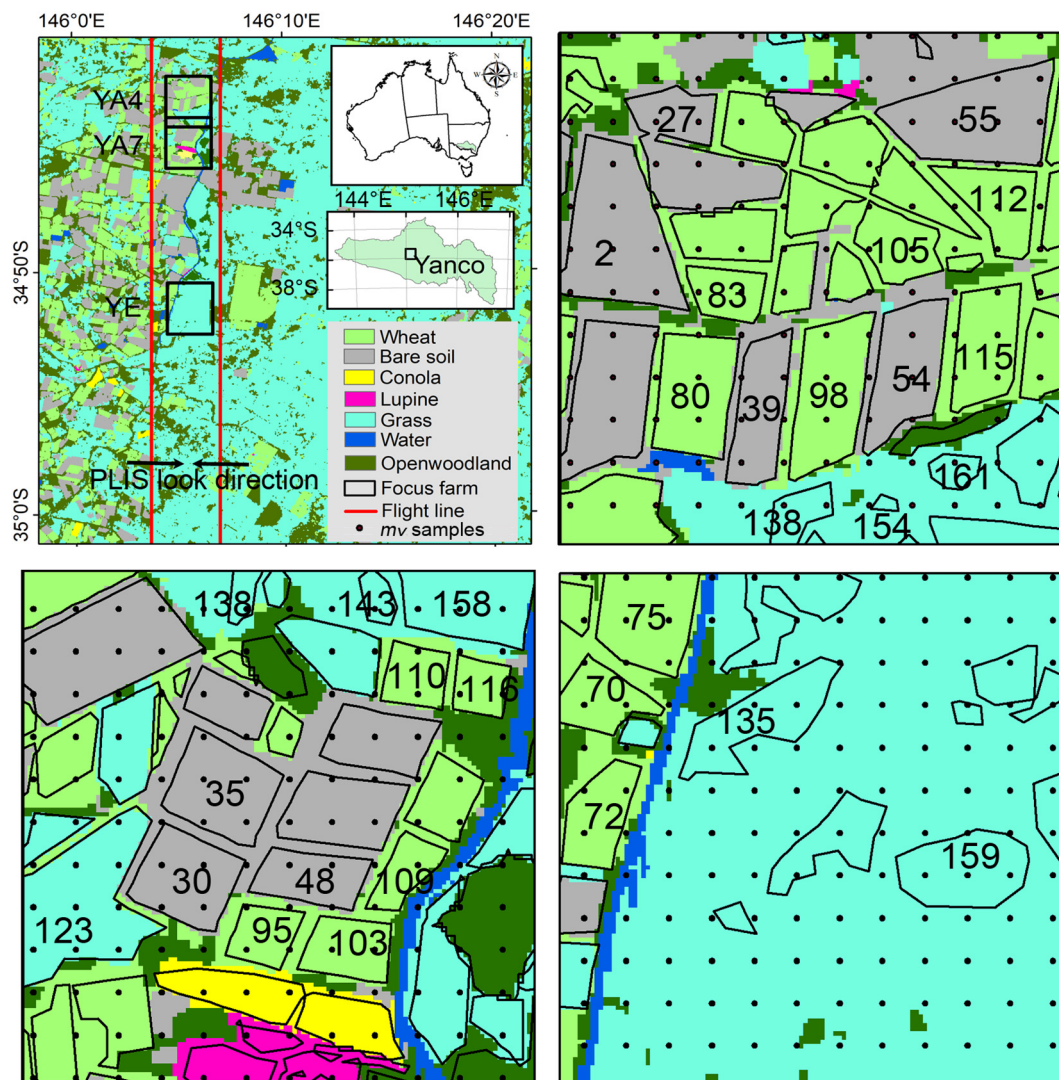


Fig. 1. Landcover and paddocks in the three SMAPEX-5 focus farms used in this study, as well as the flight and look directions of L-band airborne SAR. Focus farms are YA4 (top right), YA7 (bottom left) and YE (bottom right). The paddocks with ID are those with soil roughness and/or vegetation measurements as given in Table 1. Three soil moisture measurements were made at each black point.

of geophysical parameters to be determined, and the uncertainties of calibration and subpixel heterogeneity. Consequently, additional constraint is required, such as including more than a single SAR observation. Options include multi-frequency data (e.g., Bindlish and Barros, 2000, 2001; Pierdicca et al., 2008; Zhang et al., 2016) and/or multi-angular data (e.g., Rahman et al., 2008; Shen et al., 2013; Zribi et al., 2005; Zribi and Dechambre, 2003). While current SAR missions can provide full polarized data, unfortunately they are still unable to regularly collect multi-angular and/or multi-frequency data simultaneously, limiting the application of these methods.

The other promising strategy for operational soil moisture mapping is to use the temporal behavior of soil moisture together with other geophysical parameters. The temporal behavior of soil moisture is usually characterized by a relatively fast dry-down process following an abrupt increase from precipitation, whereas changes in soil roughness and vegetation undergo relatively smooth transition over time apart from deliberate cultivation practices. Accordingly, roughness and vegetation parameters may be considered constant for acquisitions over sufficiently short time intervals. Based on this assumption, studies have directly related the difference/ratio of multi-temporal SAR observations to soil moisture or wetness, known as change detection techniques (Balenzano et al., 2011; Notarnicola, 2014; Ouellette et al., 2017;

Wagner et al., 1999; Wickel et al., 2001). Others have used the same assumption to partly remove unknowns representing the time-variation of surface roughness and vegetation in an inversion framework (Kim et al., 2014; Kim et al., 2012a; Kim and Van Zyl, 2009; Kweon and Oh, 2014; Mattia et al., 2009; Pierdicca et al., 2010). Moreover, ancillary data or a priori information is commonly integrated to improve the retrieval accuracy; e.g. soil moisture from hydrological models (Mattia et al., 2009), passive microwave data (Kim and Van Zyl, 2009) and vegetation water content (Kim et al., 2014; Pierdicca et al., 2010). Currently, the main limitation of these multi-temporal methods is the availability of radar data with a short time lag and similar radar configuration (Balenzano et al., 2011; Kornelsen and Coulibaly, 2013).

Making the situation even more challenging, present SAR missions commonly operate with alternating imaging modes in ascending and descending orbits, resulting in changes of both incidence angle and polarization in time. For example, the SAOCOM constellation and ALOS-2/PALSAR-2 operate at both ascending and descending orbits with multiple imaging modes alternating in time, namely, ScanSAR, StripMap and Spotlight (Giraldez, 2003; Rosenqvist et al., 2014). Consequently, a much longer time interval than the reported satellite revisit is required for acquiring multi-temporal data with the same radar configuration. The use of multi-angular time series data with

Table 1

Available roughness and vegetation measurements of the paddocks in three SMAPEX-5 focus farms used in this study.

| # | Landcover | Vegetation parameters | | | | Soil surface parameters | | | Cultivation DOY |
|-----|-----------|--------------------------|------------|-------------|---------------------|-------------------------|----------------------------------|---|-----------------|
| | | VWC (kg/m ²) | Height (m) | Radius (mm) | Elevation angle (°) | Row direction | H _R ^a (cm) | L _c /H _R ^a | |
| 2 | Bare | - | - | - | - | 90 | 1.94(8.66) | 6.82(2.44) | 264 |
| 27 | Bare | - | - | - | - | - | 1.22 | 14.53 | |
| 30 | Bare | - | - | - | - | 28 | 2.76(6.33) | 5.13(2.95) | 269 |
| 35 | Bare | - | - | - | - | 28 | 1.61(5.54) | 8.24(3.65) | |
| 48 | Bare | - | - | - | - | 90 | 2.12(6.30) | 7.76(3.20) | 269 |
| 54 | Bare | - | - | - | - | 10 | - | - | 263 |
| 55 | Bare | - | - | - | - | - | 1.50 | 6.98 | |
| 70 | Wheat | 2.00 | 0.46 | 1.42 | 25 | - | - | - | |
| 72 | Wheat | 2.78 | 0.47 | 1.49 | 30 | - | 1.60 | 7.44 | 269 |
| 75 | Wheat | 2.93 | 0.77 | 1.50 | 25 | 90 | 1.12(4.05) | 6.58(4.99) | |
| 80 | Wheat | 2.21 | 0.62 | - | - | 10 | 1.95(3.71) | 14.20(5.83) | |
| 83 | Wheat | 3.11 | - | - | - | 90 | 0.87(4.03) | 7.19(6.51) | |
| 95 | Wheat | 2.48 | 0.72 | - | - | 90 | 1.45(2.58) | 5.61(4.59) | |
| 98 | Wheat | 2.69 | 0.70 | - | - | 10 | - | - | |
| 103 | Wheat | 2.82 | 0.74 | - | - | 90 | 1.54(2.83) | 6.95(5.34) | 269 |
| 105 | Wheat | 1.72 | 0.60 | 1.02 | - | - | 0.91 | 20.93 | |
| 109 | Wheat | 2.32 | 0.71 | - | - | - | - | - | 269 |
| 110 | Wheat | 1.17 | 0.61 | - | - | - | - | - | 269 |
| 112 | Wheat | 1.60 | 0.66 | 1.00 | 20 | 90 | 2.46(3.12) | 9.16 (9.91) | |
| 115 | Wheat | 3.72 | 1.05 | 1.63 | 20 | 10 | 1.01(2.94) | 11.30(6.49) | |
| 116 | Wheat | 2.81 | 0.67 | 1.51 | 22.5 | 90 | 1.06(2.76) | 7.24(4.98) | 269 |
| 117 | Wheat | 2.93 | 0.60 | - | - | 55 | 1.18(2.38) | 2.94(6.74) | |
| 135 | Grass | 0.69 | 0.32 | - | - | - | 1.20 | 17.86 | |
| 138 | Grass | 0.73 | 0.30 | - | - | - | 1.21 | 7.12 | |
| 143 | Grass | 1.62 | 0.43 | - | - | - | 0.71 | 14.98 | |
| 154 | Grass | 1.22 | - | - | - | - | 0.71 | 14.98 | |
| 158 | Grass | 0.92 | - | - | - | - | 0.71 | 14.98 | |
| 159 | Grass | 0.53 | 0.30 | - | - | - | 0.96 | 18.21 | |
| 161 | Grass | 0.98 | 0.33 | - | - | - | 1.15 | 20.34 | |

-: not available.

^a Roughness along (perpendicular) to row structure for paddocks with periodic surface.

different polarizations is therefore questionable in change detection techniques, while scattering models that accurately describe the angular dependence of SAR data are needed for multi-temporal inversion methods.

To overcome these challenges, this study proposes a multi-angular time series method for soil moisture mapping from a sequence of L-band SAR data, e.g. the joint data sets of PALSAR-2 and the SAOCOM constellation. The method applies the assumption of constant soil roughness and vegetation over the retrieval period with the main difference being i) multi-angular LUTs were built using the physical-based NMM3D and distort Born approximation (DBA, Lang and Sighu, 1983), meaning no incidence angle normalization and/or cumbersome tuning of radar-specific configuration parameters is required, and 2) a priori information of dry-down soil moisture is integrated into a genetic algorithm (GA) based inversion of LUTs to partly remove the uncertainties in calibration, speckle noise removal and forward models. The method was evaluated using the multi-angular airborne L-band data collected during the fifth Soil Moisture Passive Active Experiment (SMAPEX-5, Ye et al., 2016). The effects of data time interval and polarization combinations on retrieval accuracy were also investigated to guide the use of the method in future applications.

2. Data set and pre-processing

The SMAPEX-5 was carried out in the Australian Spring (7th – 27th September 2015) for the purpose of in-orbit calibration and validation of the NASA Soil Moisture Active Passive (SMAP) mission (Ye et al., 2016). The SMAPEX-5 study site is a semi-arid cropping and grazing area near the Yanco agricultural institute, located in the center of the Murrumbidgee River catchment Australia. Three 3 km × 3 km focus farms (YA4, YA7 and YE) of SMAPEX-5 were selected, with the main landcover being winter wheat, grass, bare soil and open wood land

(Fig. 1). Since the tree coverage in the open wood land was < 5% (~2000–3000 trees/km²), the open wood land was also treated as grass land for soil moisture retrieval here. The boundaries of paddocks (fields) were delineated using visual interpretation according to the homogeneity of landcover and the availability of ground measurements. A total of 69 individual paddocks were extracted, accounting for 48% of the three focus farms. Notably, the boundaries were only used for analyzing the results at the paddock scale and soil moisture retrieval at the pixel scale was performed for the whole research area, with the water bodies removed before retrieval.

Throughout the campaign, intensive soil moisture measurements (m_v) were made on September 9th, 14th, 19th, and 24th for YA4 and YE, and on 11th, 17th, 22th, and 27th for YA7 using the Hydraprobe Data Acquisition System (HDAS, Merlin et al., 2007). Measurements were made on a north-south oriented grid with a spacing of 250 m, with three point-based soil moisture measurements made within a 1 m radius at each sampling location (the black points in Fig. 1) to account for small scale soil moisture variability. At the end of each intensive sampling day, three gravimetric soil samples representing low, medium, and high soil moisture status within each sampled 3-km focus area were collected for calibration of the HDAS. The comparison between HDAS and gravimetric soil samples showed a root mean square difference (RMSD) of better than 0.04 m³/m³. A moderate rainfall of ~18 mm (measured at the Yanco agricultural institute) occurred prior to the experiment, resulting in m_v values of larger than 0.4 m³/m³ followed by a three-week dry down period to values of below 0.1 m³/m³.

Roughness was measured along a 3 m segment using a pin profiler in two orthogonal directions, north-south and east-west, or along and across rows in the case of a row structure. At least two measurements were made within the paddock to characterize spatial variability in surface roughness. Repeat measurements were made at the beginning and end of the campaign at paddocks #2, #48, #55, #105, #161,

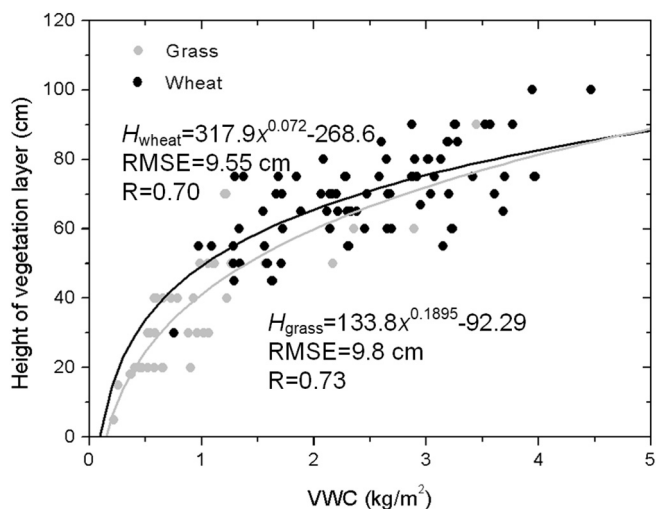


Fig. 2. Fitted relationship between vegetation water content and vegetation height.

#103, and #159, showing time-invariant roughness over the entire period of SMAPEX-5, except for those with cultivation activities. The surface root mean square height (H_R) and correlation length (L_C) were calculated from each 3 m long surface height profile extracted from digital photographs. All measurements for a paddock were then averaged (listed in Table 1), with the intra-paddock standard deviation of H_R ranging from 0.10 to 0.34 cm. In general, wheat and bare soil paddocks had a wide range of roughness with large values observed on those with furrows due to tillage.

Intensive vegetation sampling, such as plant height, orientation, and VWC, was carried out over grass and wheat paddocks between the soil moisture sampling days. The wheat had spatially varying VWC values ranging from 1.17 to 3.72 kg/m², which is mainly caused by the spatial heterogeneity of plant density (120–370/m²) and height (0.35–1.0 m). Allometric relationships between VWC and height for grass and wheat were fitted (Fig. 2) using ground measurements of the whole SMAPEX-5 area. No clear tendency of VWC values was observed, but there were significant fluctuations over time for most paddocks during the three-week period, mainly caused by the intra-paddock heterogeneity, as it was impossible to resample at exactly the same location using the destructive collection of samples for VWC estimation. Consequently, all vegetation parameters for the same location were assumed constant in time and averaged for each paddock with the average values presented in Table 1.

Eight flights were carried out coincident with soil moisture sampling dates, providing L-band (1.26 GHz) single look complex data with a spacing of 2 m × 3.75 m using the airborne Polarimetric L-band Imaging SAR (PLIS) oriented towards the West or East (Fig. 1). Consequently, radar observations of each location had two local (across track) incidence angles within 20°–50°. In this study, a multi-angular time series data set was built using data collected alternatively from the right and left sides of the aircraft, which can be treated as being similar to a series of ascending and descending orbits. The potential incidence angle difference of two successive PLIS measurements ranged from 0 to 30°, with the smallest and largest difference being at the center and boundaries respectively. This is commonly larger than the general incidence angle difference of satellite data. PLIS backscatter data were calibrated, geo-referenced, multi-looked (12 × 7 looks) and resampled to 25 m by the nearest neighbor method, with a calibration accuracy of better than 0.65 dB (RMSE) according to trihedral corner reflector and polarimetric active radar calibrator comparisons (Zhu et al., 2018).

3. Methodology

3.1. Forward models

The NMM3D (Huang and Tsang, 2012) and DBA (Lang and Sighu, 1983) were used to model backscattering of the dominant landcover types (i.e., bare soil, wheat and grass) of SMAPEX-5. In the theory of DBA, the total backscattering coefficient σ_{pq}^{total} at polarization pq (HH, HV, VH or VH for PLIS data) can be qualitatively decomposed into a sum of three dominant components according to:

$$\sigma_{pq}^{total} = \sigma_{pq}^{soil}(\epsilon, H_R, L_C) \exp(-2\tau(V)) + \sigma_{pq}^{db}(\epsilon, H_R, L_C, V) + \sigma_{pq}^{vol}(V), \quad (1)$$

where $\sigma_{pq}^{soil} \exp(-2\tau)$ is the two-way attenuated scattering from the soil surface with τ denoting the vegetation opacity along the signal path; σ_{pq}^{vol} and σ_{pq}^{db} are the volume scattering and scattering interaction (known as double-bounce scattering) between soil surface and vegetation, respectively. The commonly used first-order radiative transfer models (e.g., Ulaby et al., 1990) share a similar form to Eq. (1), with the main difference being the enhanced double-bounce scattering in the DBA because of the full simulation in coherent scattering (Tsang et al., 1985). In principle, the double-bounce scattering has a significant contribution on the cross-polarization (HV or VH) backscatter resulting in considerable sensitivity to the soil moisture as observed in SMAPEX-5 at L-band (Zhu et al., 2019), while it contributes little to the HH and VV polarization backscatter, depending on the incidence angle, soil moisture, VWC and roughness. For C- and X-band, the double-bounce is greatly enhanced for co-polarization, with experimental observations available in Brown et al. (2003). The volume scattering is commonly negligible for all polarizations at L-band, being > 10 dB lower than soil surface scattering in this study.

The quantity ϵ in Eq. (1) is the relative permittivity of the near-surface soil as a function of soil moisture. H_R and L_C are the root mean square height and the correlation length of soil surface roughness, respectively, and V is a bulk vegetation parameter describing the vegetation layer. For soil moisture inversion, Eq. (1) must be simplified and parameterized in terms of fewer soil and vegetation parameters, considering the limited number of independent radar observations available and the drastically increased complexity of the inversion problem with more than three unknown geophysical parameters. Consequently, only the real part (ϵ_r) of the relative permittivity was used, with the corresponding imaginary part being a constant between 1 and 4.5 (Kim et al., 2012a).

Rough soil surfaces were assumed to follow a stationary Gaussian random process with an isotropic exponential correlation function, which is widely acknowledged to match natural surfaces well (Ulaby et al., 2014). However, directional row or tillage features were observed over several paddocks (Table 1), with more comprehensive descriptions of roughness or multi-scale models (e.g., Blaes and Defourny, 2008; Mattia, 2011; Monsivais-Huertero et al., 2018; Wegmüller et al., 2011; Zribi et al., 2002) being undoubtedly more suitable for these paddocks. Additional parameters are required in this case, leading to an increasingly complex problem. Fortunately, previous studies (Champion and Faivre, 1996; Joseph et al., 2010) have shown that effective isotropic roughness values can be used to account for the surface scattering of periodic features. Those effective roughness values were either determined via calibration of the forward models (Baghdadi et al., 2004; Baghdadi et al., 2002; Joseph et al., 2010; Lievens et al., 2011) or directly retrieved together with soil moisture in an iterative manner (Bai et al., 2016). Since the effective roughness was dependent on the incidence angle, polarization and frequency (Lievens et al., 2011; Zhu et al., 2016), the calibration process is not suitable in this study, because of the time-varying incidence angle, with the effective roughness being retrieved together with the soil moisture. Consequently, H_R was selected as the only independent effective roughness parameter, with the corresponding L_C values assumed to be $10H_R$. The use of this

Table 2

Parameters used in building look up tables; $U(a, b)$ denotes a uniform distribution ranging from a to b ; and $N(a, b)$ is a normal distribution with a mean of a and a standard deviation of b .

| Parameter | Wheat | Grass | Bare |
|--------------------------|-----------|-----------|-------|
| α (°) | U(0, 360) | U(0, 360) | – |
| β (°) | N(30, 4) | N(60, 15) | – |
| M_{veg} | 0.75 | 0.65 | – |
| r (mm) | 1.4 | 1.2 | – |
| VWC (kg/m ²) | 0.5–5 | 0.1–3 | – |
| ϵ_r | 3–30 | 3–30 | 3–30 |
| H_R (cm) | 0.5–4 | 0.5–4 | 0.5–4 |
| θ (°) | 20–50 | 20–50 | 20–50 |

constant ratio was based on the poor performance of using the observed L_c values in the IEM forward simulations of the same research area (Zhu et al., 2016), the negligible error ($< 0.015 \text{ m}^3/\text{m}^3$) expected by this assumption (Kim et al., 2012a), and the need to limit the number of independent unknown parameters.

Both grass and wheat were simplified as a layer of randomly distributed cylinders. These cylinders are assumed to be homogeneous, lossy, uniformly distributed with consistent size and volumetric water content in each radar illumination grid. A number of parameters are required in the DBA to model the backscatter from a cylinder-like vegetation layer (Huang et al., 2017a), including the length l (m), radius r (m), azimuth angle α (°), elevation angle β (°), density n (1/m²) and volumetric water content M_{veg} (m³/m³) of the cylinders. Among these, n and l showed large spatial variations as mentioned above, with other vegetation parameters being relatively homogenous spatially (Table 1). For inversion, only the VWC was used to represent the whole vegetation layer, as in previous studies (e.g., Huang et al., 2017a; Joseph et al., 2010; Kim et al., 2014). Specifically, the r , α , β and M_{veg} were set as spatially uniform in the forward simulation and directly determined using the ground measurements summarized in Table 2. The heterogeneous parameters l and n were represented by VWC through the fitted allometric relationships (Fig. 2) and the equation:

$$n = \frac{VWC}{\pi r^2 l \rho M_{veg}}, \quad (2)$$

where ρ is the density of water ($\sim 1000 \text{ kg/m}^3$).

After the above simplification and parameterization, Eq. (1) can be written as:

$$\sigma_{pq}^{total} = \sigma_{pq}^{soil}(\epsilon_r, H_R) \exp(-2\tau(VWC)) + \sigma_{pq}^{db}(\epsilon_r, H_R, VWC) + \sigma_{pq}^{vol}(VWC), \quad (3)$$

requiring three independent unknowns (ϵ_r , H_R , VWC) for forward prediction. The NMM3D was used to calculate σ_{pq}^{soil} and the coherent reflectivity of the soil surface that is required in the calculation of σ_{pq}^{db} , while τ and σ_{pq}^{vol} were estimated using the theory of DBA. More details about the estimation of these terms can be found in Huang et al. (2017a). Since both the NMM3D and DBA are computationally intensive, LUTs were precomputed as representations of forward backscattering at L-band (1.26 GHz) rather than directly integrating models to an inversion framework. A summary of the parameters used for building these LUTs are listed in Table 2; the ϵ_r ranged from 3 to 30, covering the very dry ($\sim 0.03 \text{ m}^3/\text{m}^3$) to very wet ($\sim 0.42 \text{ m}^3/\text{m}^3$) soil experienced in the Yanco area (Dobson et al., 1985); the H_R ranged from 0.5 to 4 cm, covering the validity range of all paddocks except the roughness measured across the row structure in several paddocks (#2, #27, #30, #48, #75 and #83) during SMAPEX-5 (Table 1); and the VWC for wheat and grass ranged from 0.5 to 5 kg/m² and 0.1–3 kg/m², respectively.

Limited by the NMM3D's computational requirements, only six H_R nodes (0.5, 1, 1.5, 2, 3, and 4 cm) and seven ϵ_r nodes (2.8, 4, 5.5, 9, 15, 22 and 30) were used for the initial LUTs at an incidence angle of 20°,

30°, and 50°, while an additional H_R node of 5 cm was included for 40° (Kim et al., 2012a). These LUTs in dB were then interpolated in terms of dB with 256 nodes at H_R and ϵ_r at 31 equal incidence angles from 20° to 50°, using a cubic spline function. The steps in H_R and ϵ_r were $\sim 0.014 \text{ cm}$ and ~ 0.106 respectively, resulting in interpolation errors $< 0.05 \text{ dB}$ (Kim et al., 2012a). The bare soil LUTs were then used as the input to Eq. 3 for generating vegetation LUTs. The initial LUTs for grass and wheat had a resolution of 0.05 kg/m^2 in VWC, with seven incidence angles ranging from 20° to 50° with an interval of 5°. Those LUTs were then interpolated to 31 incidence angle specific cubes with the VWC also being interpolated into 256 nodes. A comparison over 1000 random combinations of VWC, ϵ_r , H_R and θ showed that the maximum difference between interpolated LUTs and NMM3D-DBA is $< 0.2 \text{ dB}$.

3.2. Multi-temporal retrieval constrained by a dry down assumption

Three unknowns (ϵ_r , H_R , VWC) need to be determined in Eq. (3) for soil moisture retrieval, with the full-polarized PLIS data (HH, HV or VH, VV) being not always sufficient in single-radar-acquisition retrieval (also known as snapshot retrieval), considering the radar measurement noise. Similar to earlier studies using multi-temporal data (e.g., Balenzano et al., 2011; Kim et al., 2012a), the assumption of time-invariant roughness and vegetation was applied to remove the unknowns describing the temporal evolution of roughness and vegetation. Given a time series of N PLIS acquisitions sequentially collected at times t_1, t_2, \dots, t_N , $3N$ independent measurements are available without considering the dependence among polarizations. $N + 1$ unknowns need to be determined for bare soil consisting of $N \epsilon_r$ (i.e., $\epsilon_{r1}, \epsilon_{r2}, \dots, \epsilon_{rN}$) and one H_R , while an extra parameter of VWC needs to be derived for vegetated areas. This makes the soil moisture retrieval a well-constrained inversion for most operational polarimetric SAR missions, e.g. PALSAR-2, because either two dual-polarized or one full-polarized acquisition are acquired in time series ensuring at least $N + 2$ measurements.

The general formulation therefore is to minimize the cost function:

$$f(\epsilon_{r,1}, \epsilon_{r,2}, \dots, \epsilon_{r,N}, H_R, VWC) = \sqrt{\frac{1}{N} \sum_{i=1}^N w_{pq,i} (\sigma_{pq,i}^0 - \sigma_{pq,LUT}^0(H_R, \epsilon_{r,i}, VWC, \theta_i))^2}, \quad (4)$$

where $\sigma_{pq,i}^0$ and $\sigma_{pq,LUT}^0$ are the backscattering coefficients in dB from observation and LUTs, respectively. The subscript i denotes the time sequence from 1 to N , and the weight $w_{pq,i}$ accounts for the differing error of the LUTs and radar observations. The main sources of this error include:

- i) Speckle. SAR data inherently suffer from speckle noise, originated by the SAR system's coherent nature (Ulaby et al., 2014). The speckle noise can be partly removed by the multi-look operation at the expense of spatial resolution (Thoma et al., 2006), with the available SLC pixels being different among imaging modes and varying across the swath. Consequently, it is impossible to multi-look the data with the same number of looks for a consistent retrieval grid, resulting in different levels of residual speckle noise.
- ii) Calibration uncertainty. Time series data collected by different imaging modes may have inconsistent calibration and geometric accuracy, e.g. the difference between PALSAR-2 ScanSAR and StripMap mode reported by Shimada et al. (2009). A similar difference was also observed among different beams of the COSMO SkyMed and among different X-band missions (Pettinato et al., 2013).
- iii) Forward model error. A forward model could have a different accuracy at different incidence angles and polarizations. The currently available surface scattering models are prone to larger errors at higher incidence angles (Mancini et al., 1999; Mattia et al., 2006). The NMM3D-DBA used in this study may also have error imbalance

among different incidence angles. Huang et al. (2017b) has demonstrated a significant overestimated attenuation of the DBA at C-band, which can be worse for VV polarization at larger incidence angles than for other radar configurations.

Differing from the retrieval methods that use time series data with the same radar configuration (e.g., Kim et al., 2012a), none of the three sources can be accurately modeled in this study because of the time varying incidence angle, polarization and number of available SLC pixels. In order to keep the method as general as possible, it is not suitable to have an assumption of w_{pq} in Eq. (4). Hence, the weights were taken as uniform for all channels and a priori information on the temporal soil moisture trend was imposed:

$$30 \geq \epsilon_{r,i} \geq \epsilon_{r,i+1} \geq 3, \quad (i < N), \quad (5)$$

denoting a drying down process during the period of radar observations. This can be guaranteed for periods following a rainfall event like that prior to SMAPEX-5. In addition, rainfall and/or irrigation events can be easily identified due to the significant increase of backscattering coefficients in all polarizations, following the procedure outlined in (Zhu et al., 2019). With this constraint, the effect of anomaly fluctuations in time series caused by non-surface factors is expected to be partly removed.

A genetic algorithm (GA) was used to find the optimal solution of Eq. (4), because of its efficiency to search large spaces, low risk of reaching a local optimum (Gen and Cheng, 2000) and its convenience to integrate with constraints. Fig. 3 shows the flowchart of the proposed GA-based retrieval method. The inputs include the LUTs and time series PLIS data, with the corresponding landcover map used to determine the LUT type (bare soil, grass, wheat). The method starts from the generation of 20 random solutions (known as chromosomes in GA), with each solution consisting of N unknown values of ϵ_r , and one unknown value of H_R and VWC. An 8-bit binary was used to encode each unknown parameter with an example of ϵ_r included in Fig. 3. Consequently, the length of each solution was $8 \times (N + 1)$ bits and $8 \times (N + 2)$ bits for bare soil and vegetated areas, respectively. These solutions were then adaptively optimized using three genetic operations

(selection, crossover, and mutation) to minimize the cost function (Eq. (4)); please refers to Gen and Cheng (2000) for more details about genetic operations. Specially, the dry down constraint was integrated as a pre-selection step, discarding solutions not satisfying Eq. (5). A maximum iteration number of 100 was set. The $N \epsilon_r$ values of the optimal solution was finally converted to $N m_v$ values using the Dobson relationship between m_v and ϵ_r (Dobson et al., 1985).

For a comprehensive evaluation, the snapshot method based on the same LUTs was used for comparison, which retrieves soil moisture from each radar acquisition independently by minimizing:

$$f(\epsilon_r, H_R, VWC) = \sqrt{(\sigma_{HH}^0 - \sigma_{LUT,HH}^0)^2 + (\sigma_{HV}^0 - \sigma_{LUT,HV}^0)^2 + (\sigma_{VV}^0 - \sigma_{LUT,VV}^0)^2}/3, \quad (6)$$

where the retrieved H_R and VWC can be different over time. Moreover, to show the effect of a dry down constraint, the step using Eq. (5) in Fig. 3 was removed for comparison.

4. Results

4.1. Evaluation of forward model

The LUTs built by NMM3D-DBA were evaluated using the PLIS observations and ground samples over the paddocks containing roughness and VWC observations. The model σ^0 were first calculated for each m_v sample and then averaged for each paddock. The roughness values measured along the row structure were used for paddocks #2, #30 and #48, because their average roughness values are out of the range of bare soil LUTs (0.5–4 cm). Fig. 4 shows the predicted σ^0 in dB versus the PLIS observations over bare soil, grass and wheat.

The co-polarizations (HH and VV) achieved the best performance over bare soil, followed by the grass and wheat. The root mean square error (RMSE) for all land cover types (1.6–3.2 dB) were marginally larger than those reported in other studies using the same models, which are ~1.5 dB for bare (Huang et al., 2010), 1.8 dB for grass (Kim et al., 2014), and 1.1–1.7 dB for wheat (Huang et al., 2017a). One

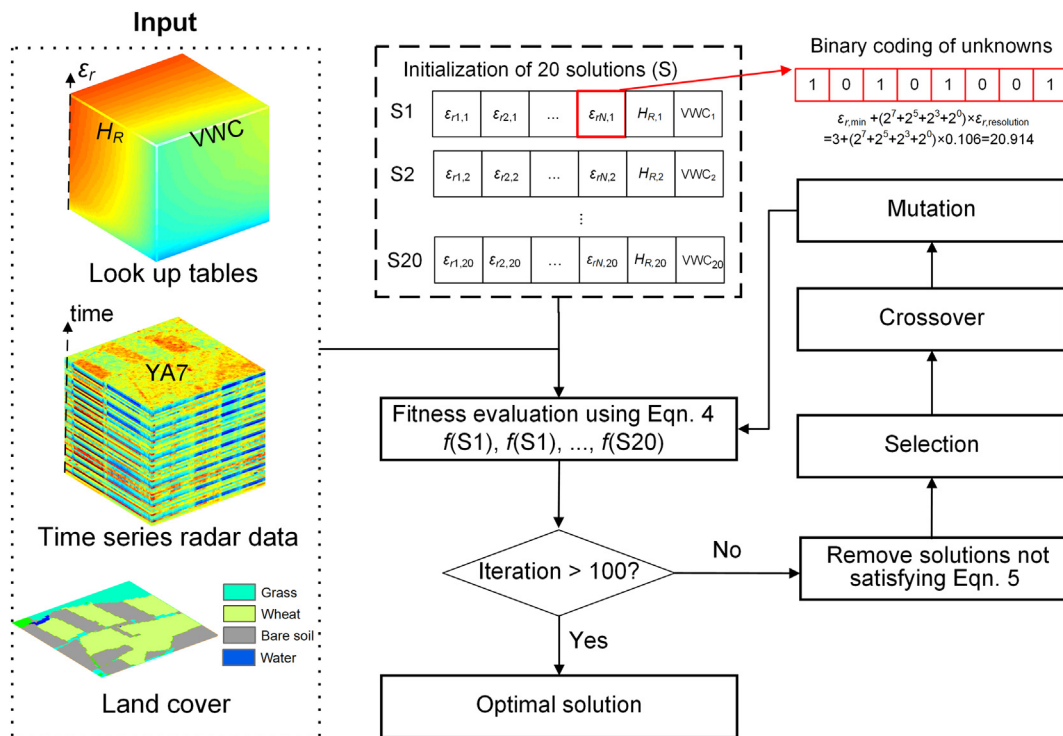


Fig. 3. Flowchart of the soil moisture retrieval method.

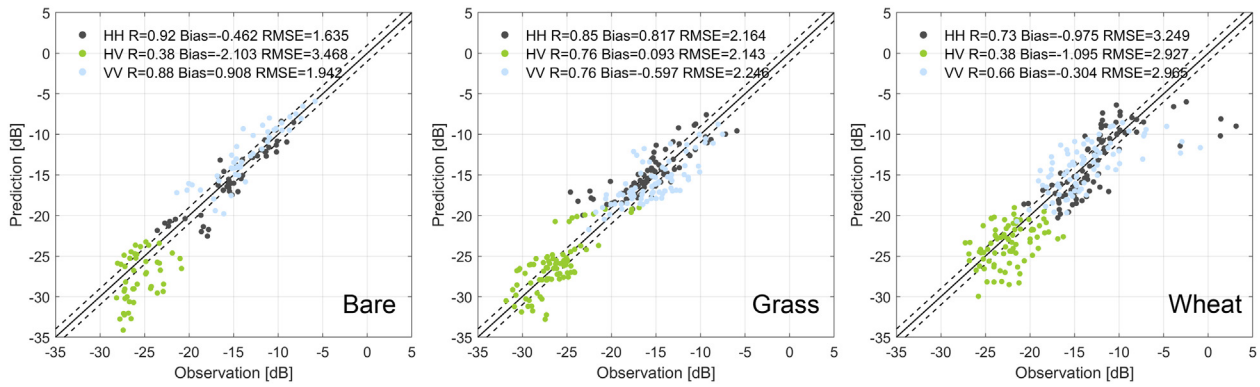


Fig. 4. Comparison of forward NMM3D-DBA σ^0 and PLIS multi-angular observations at the paddock scale (~0.1–0.5 km). The dash lines denote the ± 1 dB offset. R refers to the Pearson correlation coefficient.

reason for the difference is the periodic row structures observed in several paddocks. For example, significantly larger co-polarized σ^0 were observed at paddock #80 (wheat) which was ploughed nearly perpendicular to the radar look directions. After removing these paddocks, the RMSE for wheat decreased to 2.1 dB (HH), 2.3 dB (VV) and 2.8 dB (HV). The effect of surface row structure on radar observations is well documented (Blanchard and Chang, 1983; Champion and Faivre, 1996; Ulaby and Bare, 1979; Zribi et al., 2002), with the co-polarized σ^0 observed perpendicular to row structure being up to 10 dB larger than those observed with parallel row direction at L-band (Ulaby and Bare, 1979). Observations from other azimuth angles also have a relatively larger σ^0 compared to the parallel direction, but with a limited difference when the azimuth angle difference (θ_a) between the incident wave and row direction was $< 60^\circ$ (Blanchard and Chang, 1983). This is consistent with the σ^0 observed at other ploughed paddocks in the research area whose θ_a ranged from 0 to 62° . The predicted σ^0 of these paddocks, based on average or along row direction roughness, matched approximately the observed σ^0 having a difference of < 4 dB. Notably, this does not mean that the isotropic roughness assumption and the fixed L_c/H_R ratio of 10 accurately describes the periodic soil surface, but rather indicates that the roughness values used in the forward evaluation were close to the perceived effective roughness values for those paddocks.

A further investigation on the angular dependence of forward model performance at HH is depicted in Fig. 5, with the results for HV and VV

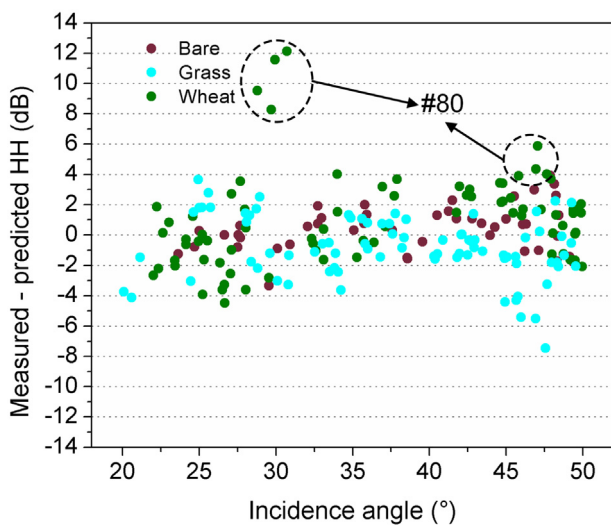


Fig. 5. The difference of measured and predicted σ^0 at HH polarization versus incidence angle. The circled points belong to paddock #80, ploughed nearly perpendicular to the radar look direction.

being similar. In general, no clear angular pattern was observed for all three landcover types, showing the reliability of the angular effect modeling. Different angular behavior was observed for paddock #80, with the PLIS observations being 8–12 dB and 4–6 dB higher than the model predictions at incidence angles of ~ 30 and 48° respectively. Similar results were observed by Ulaby et al. (2014) and Zribi et al. (2002) for 3.25 GHz.

4.2. Retrieval results

Eight full polarized images with the look direction alternating between left and right were used to simulate combined descending and ascending radar observations from space-borne sensors, to evaluate the proposed method. The multi-angular time series for a paddock with cultivation activity (Table 1) was separated into two sub-series, according to the presence of the cultivation event, with m_v retrieval carried out independently for each sub-series. The retrieved m_v (25 m resolution) at m_v sampling points against ground measured m_v are depicted in Fig. 6. Generally, an overall correlation coefficient (R) of 0.77 and a RMSE of $0.07 \text{ m}^3/\text{m}^3$ was achieved for a wide range of m_v (0.04 – $0.42 \text{ m}^3/\text{m}^3$). Different from the forward model accuracy of co-polarizations, the proposed method achieved the best results over grassland, followed by the wheat and bare soil. This may result from the poor modeling of cross-polarization at bare soil and wheat as well as the

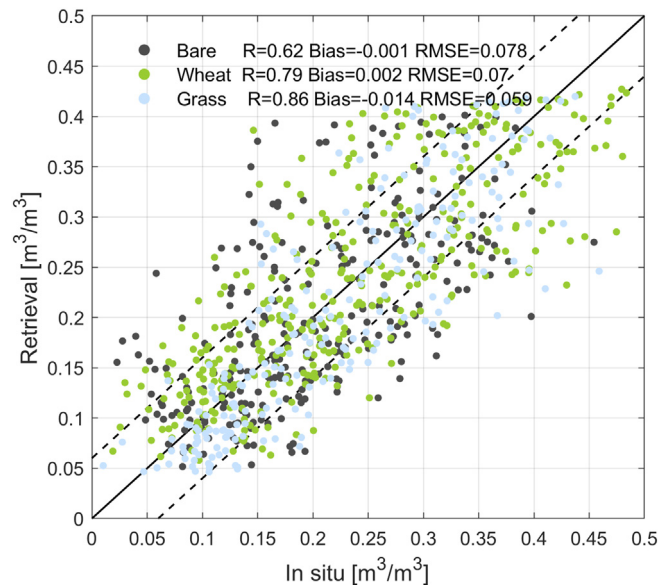


Fig. 6. In-situ versus retrieved soil moisture at the 25 m pixel scale. The dash lines denote the target accuracy of $\pm 0.06 \text{ m}^3/\text{m}^3$.

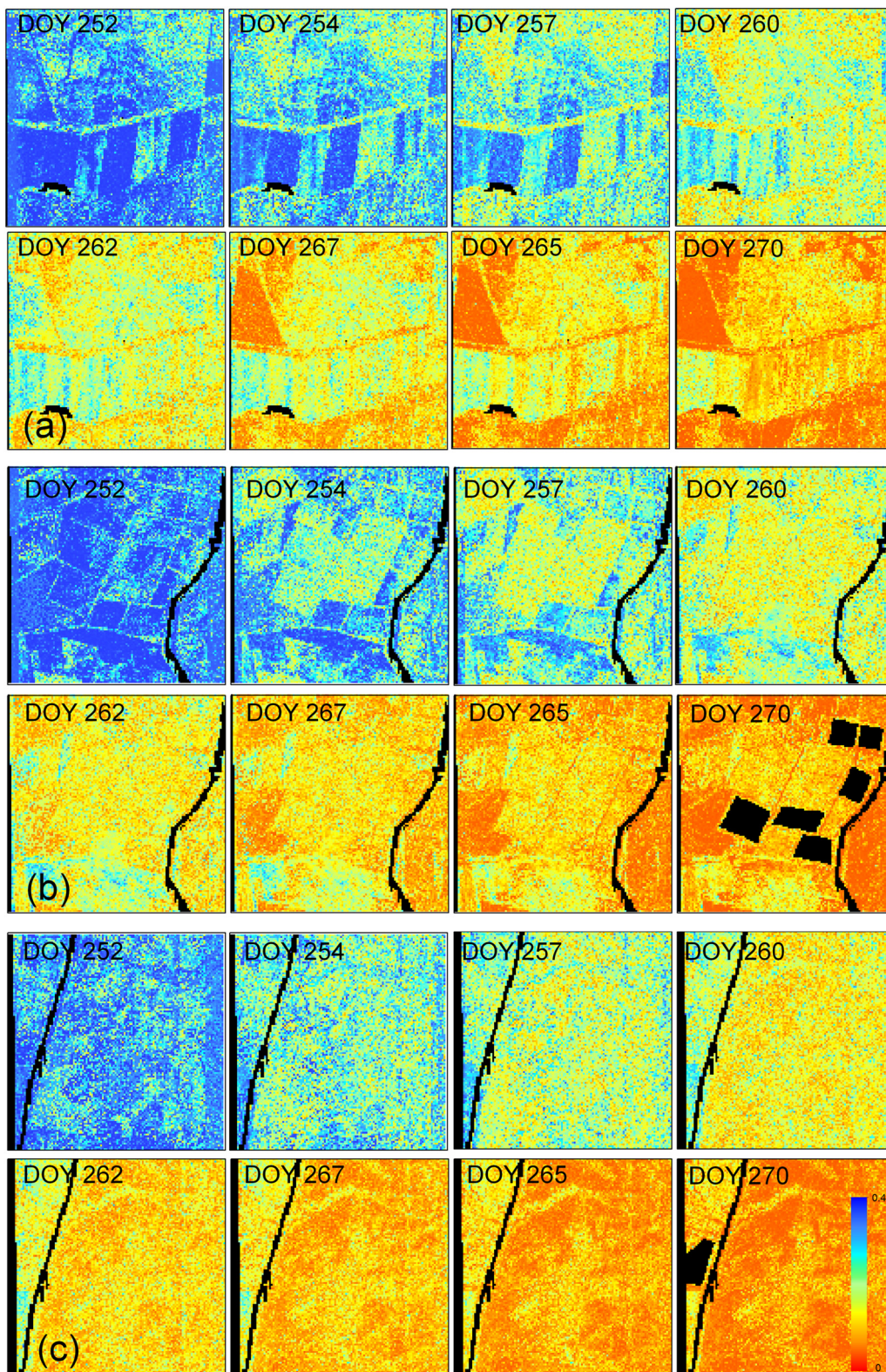


Fig. 7. Time series soil moisture maps of focus farms YA4 (a), YA7 (b) and YE (c) during the eight observation dates of the SMAPEX-5 period. The black paddocks are those with cultivation activities between DOY265 and DOY 270.

relatively simple roughness features in grassland. Underestimation was observed for high m_v conditions (larger than $0.42 \text{ m}^3/\text{m}^3$), which can be caused by i) the lower ϵ_r upper bound of LUTs ($\sim 0.42 \text{ m}^3/\text{m}^3$) compared to the wettest condition during the SMAPEX-5 period in the Yanco area, and ii) the decreased sensitivity of the radar signal to m_v at

large values.

Despite the relatively poor results compared to the $0.05 \text{ m}^3/\text{m}^3$ requirement suggested by Walker and Houser (2004) and the $0.06 \text{ m}^3/\text{m}^3$ target of SMAP radar products (Kim et al., 2012b), great spatial details of soil moisture were retained as depicted in Fig. 7. The paddocks with

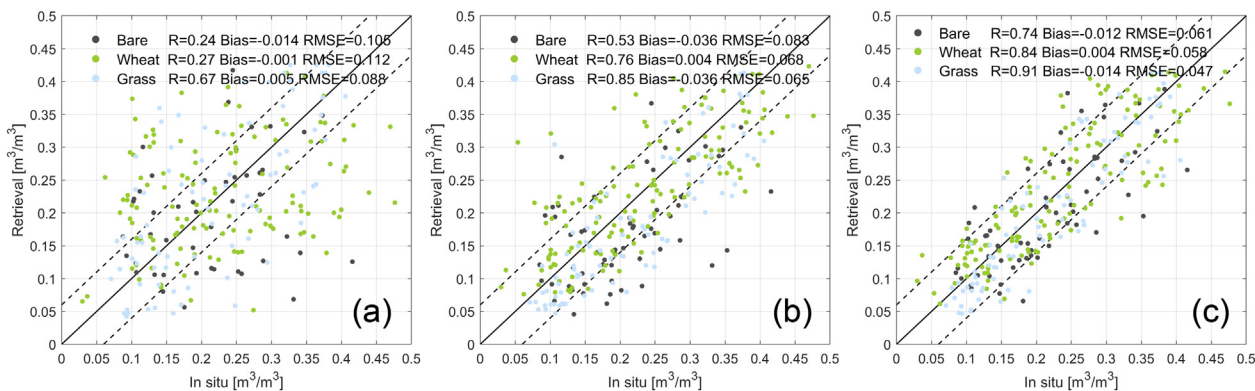


Fig. 8. Comparison of retrieved and in situ soil moisture values for multiple algorithms at the paddock scale; (a) snapshot retrieval, (b) multi-temporal retrieval and (c) multi-temporal retrieval with the dry down constraint. The dash lines denote the target accuracy of $\pm 0.06 \text{ m}^3/\text{m}^3$.

cultivation activities occurring between the last two radar acquisitions were masked for the last retrieval because only one acquisition was available after cultivation activities. The dry-down process of the SMAPEX-5 period was accurately captured over all three focus farms, with the RMSE of daily averaged m_v being 0.031, 0.017, and $0.020 \text{ m}^3/\text{m}^3$ for bare soil, grass and wheat, respectively. Spatial patterns of m_v were obtained with clear boundaries, showing relatively wetter patches for vegetated areas, particularly for the wheat farms. The m_v retrieval was also made for one canola and one lupine paddock in YA7 using the wheat LUT with acceptable results (RMSE: $0.072 \text{ m}^3/\text{m}^3$); the wheat LUT could be used because they have a similar vertical dominant structure.

The results for m_v retrieval at the paddock scale using the LUT snapshot method, the multi-temporal method without a dry down constraint and the proposed method are shown in Fig. 8 with the corresponding retrieved roughness and VWC shown in Fig. 9. It is noted that the roughness ground truth for ploughed paddocks used in Fig. 9 are those measured along the row direction, while the retrieved roughness are the effective ones. The roughness values retrieved by the snapshot algorithm were averaged over time for each paddock.

As expected, relatively poor retrieval results were achieved by the snapshot algorithm with a RMSE of $0.088\text{--}0.112 \text{ m}^3/\text{m}^3$, 1.274 cm and $1.183 \text{ kg}/\text{m}^2$ for m_v , H_R and VWC retrieval, respectively, which is ascribed to the ambiguities among soil moisture, roughness and vegetation effect on backscattering (Satalino et al., 2002) as well as the larger sensitivity of the snapshot method to noise (Kim et al., 2012a). The

impact of these uncertainties is clearly shown by the low correlation coefficients. The m_v , H_R and VWC retrieval were significantly improved using a time series retrieval even without the dry down constraint, showing a decrease in RMSE by as much as $0.03 \text{ m}^3/\text{m}^3$, 0.5 cm and $0.1 \text{ kg}/\text{m}^2$ for soil moisture, H_R , and VWC, respectively. These improvements mainly come from the reduced sensitivity of the time series retrieval to system measurement noise (Kim et al., 2012a). The m_v retrieval was further improved to an acceptable level (RMSE $< 0.06 \text{ m}^3/\text{m}^3$) by adding the dry down constraint, with slight changes in the retrieved H_R and VWC values. A possible explanation is that the dry down constraint forced slight adjustments in the H_R and VWC to ensure the soil moisture trend at the expense of a somewhat larger value of the cost function (Eq. (4)), thus removing the effect of anomaly fluctuations in time series σ^0 .

A further investigation was conducted to show the performance of the proposed method on the paddocks with row directions near-perpendicular to the radar look directions, consisting of two bare paddocks (#39 and #54) and three wheat paddocks (#80, #98 and #115). The RMSE and R of m_v retrieval were $0.056 \text{ m}^3/\text{m}^3$ and 0.826 for the bare paddocks, and $0.053 \text{ m}^3/\text{m}^3$ and 0.919 for wheat. No significant difference was found between the results of these paddocks and the other paddocks in terms of RMSE and R. This can be explained by the significantly large retrieved H_R and VWC (circled in Fig. 9). Specifically, large H_R values can result in large σ^0 from the soil surface, while the attenuation by the vegetation layer with small VWC values can be negligible. As a result, the combination of large effective H_R values and

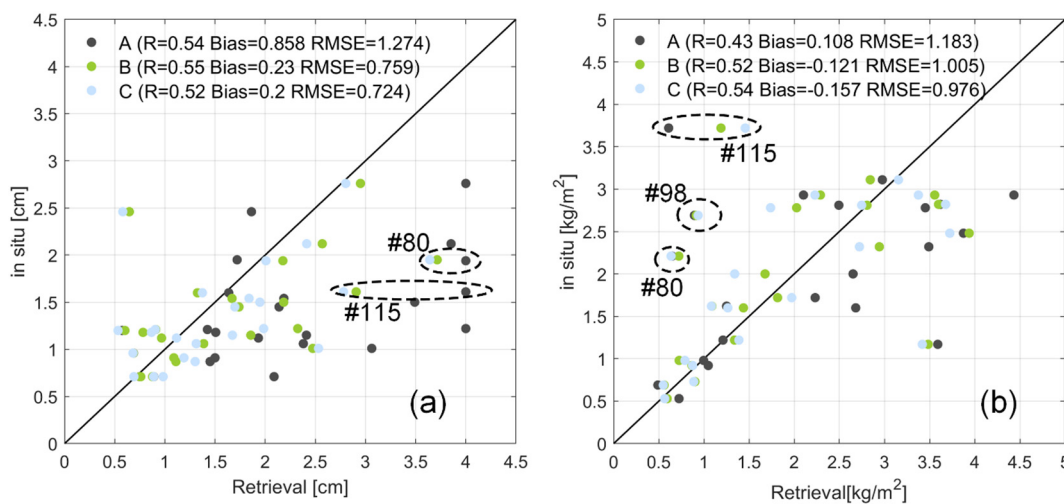


Fig. 9. Comparison of in-situ and retrieved (a) soil surface root mean square height and (b) VWC. The circled points belong to the paddocks ploughed near-perpendicular to the radar look directions with their paddock ID as labeled. A, B and C denote results of snapshot retrieval, multi-temporal retrieval and multi-temporal retrieval with the dry down constraint.

small VWC values can partly account for the strong backscattering caused by the row structure, resulting in a relatively accurate estimation of m_v . Despite the satisfactory results observed in this study, several other undesirable situations may occur. For instance, relatively accurate VWC was retrieved at the expense of overestimated m_v . Therefore, the m_v retrieval for paddocks with their row direction perpendicular to the radar look directions still needs to be further assessed using other data sets.

4.3. The effect of time interval and polarization combination

The proposed method intends to retrieve soil moisture using any given L-band time series, with potentially different polarization combinations and irregularities in time interval. The performance of the proposed method with different polarization combinations was first evaluated. Soil moisture retrieval was made at the paddock scale with different polarization combinations, including HH + HV + VV, HH + VV, HH + HV, VH + VV, HH, VV, and HV. The results are presented using the Taylor diagram (Fig. 11) which uses the standard deviation of the retrieval results, unbiased RMSE (ubRMSE) and correlation coefficient (R) between the retrievals and ground-truth data to summarize the performance of multiple algorithms in a single figure (Taylor, 2001).

In general, all combinations achieved similar ubRMSE values with the largest difference ($0.003 \text{ m}^3/\text{m}^3$) observed between the HH + HV + VV (the 'a' in Fig. 10) and single HV (the 'g' in Fig. 10) series. Fully polarized data performed slightly better than dual polarized series or single HH, HV and VV in terms of ubRMSE and R, but the difference is small. A possible explanation is that more observations introduce more uncertainties and thus cannot improve the performance for a well-constrained inversion problem. For the single polarized series, VV achieved the best results (ubRMSE: $0.056 \text{ m}^3/\text{m}^3$; R:0.858), followed by HH (ubRMSE: $0.056 \text{ m}^3/\text{m}^3$; R:0.833) and HV (ubRMSE: $0.058 \text{ m}^3/\text{m}^3$; R:0.813). Similarly, insignificant differences between VV and HH were observed in other studies (Kweon and Oh, 2014; Lievens and Verhoest, 2012; Ouellette et al., 2017; Satalino et al., 2012) with various multi-temporal algorithms, although the HH was suggested for the multi-temporal alpha approximation method at C-band (Balenzano et al., 2011).

The effect of time interval was also evaluated with the results

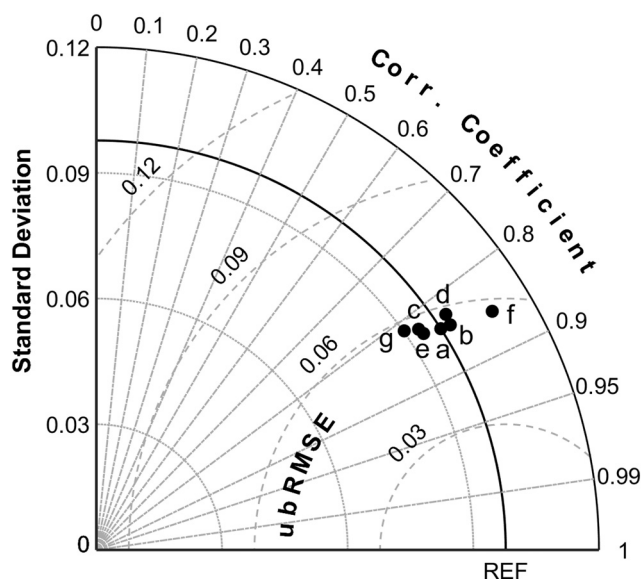


Fig. 10. Effect of polarization combinations on soil moisture retrieval when using eight multi-angular acquisitions at the paddock scale. a-f denote HH + HV + VV, HH + VV, HH + HV, VH + VV, HH, VV, and HV respectively. ubRMSE denotes the unbiased RMSE.

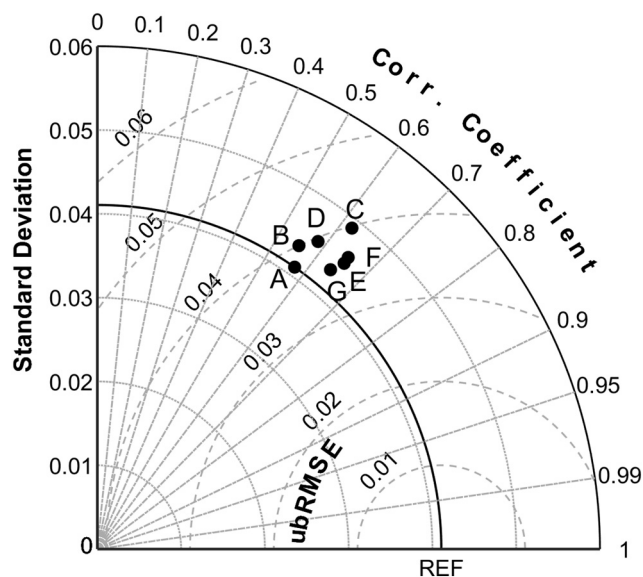


Fig. 11. Effect of time interval on soil moisture retrieval using two multi-angular acquisitions at the paddock scale. A-G denote two images with a time interval of 17, 15, 12, 9, 7, 4 and 2 days with the corresponding average soil moisture difference being 0.218, 0.181, 0.136, 0.094, 0.052, 0.015 and $0.007 \text{ m}^3/\text{m}^3$ respectively.

presented using the Taylor diagram (Fig. 11). The last PLIS acquisition of SMAPEX-5 acquired at DOY 270 was combined with acquisitions collected in the previous seven flights to form seven SAR pairs with different time intervals ranging from 2 to 17 days. The m_v retrieval was then carried out at the paddock scale using these SAR pairs respectively. As expected, retrieval with short time intervals (G, E, and F in Fig. 11) achieved relatively better results than those with long time intervals (A, B, C and D). However, the ubRMSE and R difference was $< 0.003 \text{ m}^3/\text{m}^3$ and 0.07, respectively, and the performance was not strictly consistent with the time intervals. Since the abrupt changes caused by cultivation activities were removed before m_v retrieval, this may suggest that the proposed method is insensitive to the gradual roughness and VWC changes in the SMAPEX-5 period. Importantly, results have demonstrated that the proposed method can even be used directly as a multi-angular algorithm for a period with a near-zero m_v change, e.g. the case of G (m_v difference is $0.007 \text{ m}^3/\text{m}^3$).

5. Discussion and conclusion

A time series multi-angular method was proposed for m_v retrieval from the joint time series of multiple L-band SAR missions with various imaging modes. Similar to other multi-temporal retrieval algorithms, this method also follows the assumption of time-invariant roughness and vegetation, but with an additional dry down constraint for noise reduction. In order to directly use multi-angular data, landcover specific multi-angular LUTs were built using physical scattering models (NMM3D-DBA). In contrast to less complex models like the water cloud model, which require calibration for different polarizations and even for each incidence angle, these models do not need radar-configuration-specific calibration allowing them to be used directly for other frequency bands. The performance of these LUTs was evaluated using ground measurements and airborne L-band data, showing reliable modeling of the angular behavior and a forward RMSE of 1.6–3.2 dB depending on polarizations and land cover type. However, the DBA needs several vegetation parameters, e.g. the radius of cylinders and the distribution of elevation angle, which depend on vegetation types. Consequently, the use of these LUTs for other areas needs to be assessed despite similar vegetation parameters having been used in other studies (Huang et al., 2017a). Limited by the ground measurements, in

particular the allometric relationships, the multi-angular LUTs currently only cover two vegetation types, i.e. grass and wheat, but it can be easily expanded to other vegetation types (Kim et al., 2014).

The dry down constraint used in this study provides a priori information on m_v , however the integration of similar information or assumption in soil moisture retrieval is not new (Kornelsen and Coulibaly, 2013). For instance, the m_v predicted by hydrological models (Mattia et al., 2006; Mattia et al., 2009) and the assumption of time-invariant m_v for dry or frozen conditions (Rahman et al., 2007; van der Velde et al., 2012). The merit of the dry down constraint here is its generalization such that the dry down can be guaranteed, by including a pre-processing to separate the time series into multiple sub-series, according to the presence of rainfall events or small-scale irrigations (Zhu et al., 2019). Notably, this constraint is difficult to apply for areas with frequent rainfall (e.g., tropics). In addition to the dry down constraint, the proposed method can accommodate other constraints such as increasing biomass for early stage crops.

In this paper, the soil surface was assumed to be isotropic, which is hardly true for an agricultural area, particularly in field scale application. Consequently, an effective isotropic roughness was assumed to account for the effect of periodic surface roughness features, as suggested by Champion and Faivre (1996). Both forward modeling and m_v retrieval confirmed the existence of such values in a range of cases. For paddocks with row directions perpendicular to the radar look direction, the effective isotropic roughness was much larger than that measured along the row directions, resulting in the VWC being greatly underestimated. However, limited by the number of available cases here, the validity of these statements needs to be assessed on different data sets. For operational applications, the LUT generated in this study should be extended to cover larger or smaller H_R values to account for the effect of periodic features, although these values are generally not observed in field experiments. The timing of cultivation activities and rainfall should also be considered carefully when applying the time series retrieval, with an effective solution already available (Zhu et al., 2019).

The performance of the proposed method has been comprehensively evaluated using the time series multi-angular L-band data collected during the SMAPEX-5, showing an m_v RMSE (R) of $0.07 \text{ m}^3/\text{m}^3$ (0.77) at the 25 m pixel scale and $0.056 \text{ m}^3/\text{m}^3$ (0.83) at the paddock scale. A similar m_v RMSE ($0.053 \text{ m}^3/\text{m}^3$) was reported using the SMAP radar baseline algorithm at the same research area (Kim et al., 2017). In comparison, the RMSE and R of the LUT snapshot retrieval at the paddock scale are $0.105 \text{ m}^3/\text{m}^3$ and 0.41 respectively, while the RMSE and R are $0.073 \text{ m}^3/\text{m}^3$ and 0.73 for multi-temporal retrieval without a dry down constraint. An investigation on the effect of time interval and polarization combinations has demonstrated the robustness of the proposed method using irregularly collected L-band SAR data with inconsistent polarizations. However, the performance of the proposed method should be further evaluated using satellite data (e.g., PALSAR-2 and/or SAOCOM-1), considering the different number of independent samples for multi-look airborne and satellite data. The limited number of independent samples in satellite data for the 25 m target retrieval grid is likely to have a much higher noise level than the PLIS data, with a potentially negative effect on the retrieval performance.

Acknowledgements

The PLIS was developed using funds from an Australian Research Council Linkage Infrastructure, Equipment and Facilities grant (LE0882509) while the SMAPEX-5 field campaigns were supported by an Australian Research Council Discovery Project grant (DP140100572). The authors wish to thank all the SMAPEX-5 experiment participants. The authors also acknowledge the scholarships awarded by China Scholarship Council (CSC) and Monash University to support Lijun Zhu's PhD research and visit to the University of Michigan-Ann Arbor, USA.

References

- Attema, E., Ulaby, F.T., 1978. Vegetation modeled as a water cloud. *Radio Sci.* 13, 357–364.
- Baghdadi, N., King, C., Chanzy, A., Wigneron, J., 2002. An empirical calibration of the integral equation model based on SAR data, soil moisture and surface roughness measurement over bare soils. *Int. J. Remote Sens.* 23, 4325–4340.
- Baghdadi, N., Gherboudj, I., Zribi, M., Sahebi, M., King, C., Bonn, F., 2004. Semi-empirical calibration of the IEM backscattering model using radar images and moisture and roughness field measurements. *Int. J. Remote Sens.* 25, 3593–3623.
- Baghdadi, N., Choker, M., Zribi, M., Hajj, M., Paloscia, S., Verhoest, N., Lievens, H., Baup, F., Mattia, F., 2016. A new empirical model for radar scattering from bare soil surfaces. *Remote Sens.* 8, 920.
- Bai, X., He, B., Li, X., 2016. Optimum surface roughness to parameterize advanced integral equation model for soil moisture retrieval in prairie area using Radarsat-2 data. *IEEE Trans. Geosci. Remote Sens.* 54, 2437–2449.
- Balenzano, A., Mattia, F., Satalino, G., Davidson, M.W., 2011. Dense temporal series of C- and L-band SAR data for soil moisture retrieval over agricultural crops. *IEEE J. Sel. Top. Appl. Earth Observ. Remote Sens.* 4, 439–450.
- Bindlish, R., Barros, A.P., 2000. Multifrequency Soil Moisture Inversion from SAR Measurements with the Use of IEM. *Remote Sensing of Environment*. vol. 71. pp. 67–88.
- Bindlish, R., Barros, A.P., 2001. Parameterization of vegetation backscatter in radar-based, soil moisture estimation. *Remote Sens. Environ.* 76, 130–137.
- Blaes, X., Defourny, P., 2008. Characterizing bidimensional roughness of agricultural soil surfaces for SAR modeling. *IEEE Trans. Geosci. Remote Sens.* 46, 4050–4061.
- Blanchard, B., Chang, A., 1983. Estimation of soil moisture from Seasat SAR data. *J. Am. Water Resour. Assoc.* 19, 803–810.
- Brown, S.C., Quegan, S., Morrison, K., Bennett, J.C., Cookmartin, G., 2003. High-resolution measurements of scattering in wheat canopies-implications for crop parameter retrieval. *IEEE Trans. Geosci. Remote Sens.* 41, 1602–1610.
- Champion, I., Faivre, R., 1996. The field row direction relative to the radar azimuth considered as an apparent surface roughness for smooth bare soils. *Int. J. Remote Sens.* 17, 3305–3311.
- Chen, K.-S., Wu, T.-D., Tsang, L., Li, Q., Shi, J., Fung, A.K., 2003. Emission of rough surfaces calculated by the integral equation method with comparison to three-dimensional moment method simulations. *IEEE Trans. Geosci. Remote Sens.* 41, 90–101.
- Dobson, M.C., Ulaby, F.T., Hallikainen, M.T., El-Rayes, M., 1985. Microwave dielectric behavior of wet soil-part II: dielectric mixing models. *IEEE Trans. Geosci. Remote Sens.* 35–46.
- Dubois, P.C., Van Zyl, J., Engman, T., 1995. Measuring soil moisture with imaging radars. *IEEE Trans. Geosci. Remote Sens.* 33, 915–926.
- Fung, A.K., Li, Z., Chen, K., 1992. Backscattering from a randomly rough dielectric surface. *IEEE Trans. Geosci. Remote Sens.* 30, 356–369.
- Gen, M., Cheng, R., 2000. Genetic Algorithms and Engineering Optimization. John Wiley & Sons.
- Giraldez, A.E., 2003. SAOCOM-1 Argentina L-band SAR mission overview. In: Coastal and Marine Applications of SAR Symposium.
- Huang, S., Tsang, L., 2012. Electromagnetic scattering of randomly rough soil surfaces based on numerical solutions of Maxwell equations in three-dimensional simulations using a hybrid UV/PBTG/SMCG method. *IEEE Trans. Geosci. Remote Sens.* 50, 4025–4035.
- Huang, S., Tsang, L., Njoku, E.G., Chan, K.S., 2010. Backscattering coefficients, coherent reflectivities, and emissivities of randomly rough soil surfaces at L-band for SMAP applications based on numerical solutions of Maxwell equations in three-dimensional simulations. *IEEE Trans. Geosci. Remote Sens.* 48, 2557–2568.
- Huang, H., Liao, T.-H., Tsang, L., Njoku, E.G., Colliander, A., Jackson, T.J., Burgin, M.S., Yueh, S., 2017a. Modelling and validation of combined active and passive microwave remote sensing of agricultural vegetation at L-band. *Prog. Electromagn. Res.* 78, 91–124.
- Huang, H., Tsang, L., Njoku, E.G., Colliander, A., 2017b. A new vegetation model based on numerical 3D solutions of Maxwell equations. In: 2017 IEEE International Geoscience and Remote Sensing Symposium (IGARSS). IEEE, pp. 2903–2906.
- Joseph, A., van der Velde, R., O'Neill, P., Lang, R., Gish, T., 2010. Effects of corn on C- and L-band radar backscatter: a correction method for soil moisture retrieval. *Remote Sens. Environ.* 114, 2417–2430.
- Kim, Y., Van Zyl, J.J., 2009. A time-series approach to estimate soil moisture using polarimetric radar data. *IEEE Trans. Geosci. Remote Sens.* 47, 2519–2527.
- Kim, S.-B., Tsang, L., Johnson, J.T., Huang, S., Van Zyl, J.J., Njoku, E.G., 2012a. Soil moisture retrieval using time-series radar observations over bare surfaces. *IEEE Trans. Geosci. Remote Sens.* 50, 1853–1863.
- Kim, S., Zyl, J., Dunbar, S., Njoku, E., Johnson, J., Moghaddam, M., 2012b. Algorithm Theoretical Basis Document SMAP L2 & L3 Radar Soil Moisture (Active) Data Products. Jet Propulsion Laboratory, Pasadena, California.
- Kim, S.-B., Moghaddam, M., Tsang, L., Burgin, M., Xu, X., Njoku, E.G., 2014. Models of L-band radar backscattering coefficients over global terrain for soil moisture retrieval. *IEEE Trans. Geosci. Remote Sens.* 52, 1381–1396.
- Kim, S.-B., van Zyl, J.J., Johnson, J.T., Moghaddam, M., Tsang, L., Colliander, A., Dunbar, R.S., Jackson, T.J., Jaruwatanadilok, S., West, R., 2017. Surface soil moisture retrieval using the L-band synthetic aperture radar onboard the soil moisture active-passive satellite and evaluation at Core validation sites. *IEEE Trans. Geosci. Remote Sens.* 55, 1897–1914.
- Kornelsen, K.C., Coulibaly, P., 2013. Advances in soil moisture retrieval from synthetic aperture radar and hydrological applications. *J. Hydrol.* 476, 460–489.

- Kweon, S.-K., Oh, Y., 2014. Estimation of soil moisture and surface roughness from single-polarized radar data for bare soil surface and comparison with dual-and quad-polarization cases. *IEEE Trans. Geosci. Remote Sens.* 52, 4056–4064.
- Lang, R.H., Sighu, J.S., 1983. Electromagnetic backscattering from a layer of vegetation: a discrete approach. *IEEE Trans. Geosci. Remote Sens.* 62–71.
- Lievens, H., Verhoest, N.E., 2012. Spatial and temporal soil moisture estimation from RADARSAT-2 imagery over Flevoland, the Netherlands. *J. Hydrol.* 456, 44–56.
- Lievens, H., Verhoest, N., De Keyser, E., Vernieuwe, H., Matgen, P., Álvarez-Mozos, J., De Baets, B., 2011. Effective roughness modelling as a tool for soil moisture retrieval from C-and L-band SAR. *Hydrol. Earth Syst. Sci. Discuss.* 7, 4995–5031.
- Mancini, M., Hoeben, R., Troch, P.A., 1999. Multifrequency radar observations of bare surface soil moisture content: a laboratory experiment. *Water Resour. Res.* 35, 1827–1838.
- Mattia, F., 2011. Coherent and incoherent scattering from tilled soil surfaces. *Waves Random Complex Media* 21, 278–300.
- Mattia, F., Satalino, G., Dente, L., Pasquariello, G., 2006. Using a priori information to improve soil moisture retrieval from ENVISAT ASAR AP data in semiarid regions. *IEEE Trans. Geosci. Remote Sens.* 44, 900–912.
- Mattia, F., Satalino, G., Pauwels, V., Loew, A., 2009. Soil moisture retrieval through a merging of multi-temporal L-band SAR data and hydrologic modelling. *Hydrol. Earth Syst. Sci.* 13, 343–356.
- Merlin, O., Walker, J., Panciera, R., Young, R., Kalma, J., Kim, E., 2007. Calibration of a soil moisture sensor in heterogeneous terrain. In: Oxley, L., Kulasiri, D. (Eds.), 2007 International Congress on Modelling and Simulation (MODSIM). Modelling and Simulation Society of Australia and New Zealand pp. 2604–2610.
- Monsivais-Huetero, A., Liu, P.-W., Judge, J., 2018. Phenology-based backscattering model for corn at L-band. *IEEE Trans. Geosci. Remote Sens.* 56, 4989–5005.
- Notarnicola, C., 2014. A Bayesian change detection approach for retrieval of soil moisture variations under different roughness conditions. *IEEE Geosci. Remote Sens. Lett.* 11, 414–418.
- Oh, Y., Sarabandi, K., Ulaby, F.T., 2002. Semi-empirical model of the ensemble-averaged differential Mueller matrix for microwave backscattering from bare soil surfaces. *IEEE Trans. Geosci. Remote Sens.* 40, 1348–1355.
- Ouellette, J.D., Johnson, J.T., Balenzano, A., Mattia, F., Satalino, G., Kim, S.-B., Dunbar, R.S., Colliander, A., Cosh, M.H., Caldwell, T.G., 2017. A time-series approach to estimating soil moisture from vegetated surfaces using L-band radar backscatter. *IEEE Trans. Geosci. Remote Sens.* 55, 3186–3193.
- Pettinato, S., Santi, E., Paloscia, S., Pampaloni, P., Fontanelli, G., 2013. The inter-comparison of X-band SAR images from COSMO-SkyMed and TerraSAR-X satellites: case studies. *Remote Sens.* 5, 2928–2942.
- Pierdicca, N., Castracane, P., Pulvirenti, L., 2008. Inversion of electromagnetic models for bare soil parameter estimation from multifrequency polarimetric SAR data. *Sensors* 8, 8181–8200.
- Pierdicca, N., Pulvirenti, L., Bignami, C., 2010. Soil moisture estimation over vegetated terrains using multitemporal remote sensing data. *Remote Sens. Environ.* 114, 440–448.
- Rahman, M., Moran, M., Thoma, D., Bryant, R., Sano, E., Holifield Collins, C., Skirvin, S., Kershner, C., Orr, B., 2007. A derivation of roughness correlation length for parameterizing radar backscatter models. *Int. J. Remote Sens.* 28, 3995–4012.
- Rahman, M., Moran, M., Thoma, D., Bryant, R., Collins, C.H., Jackson, T., Orr, B., Tischler, M., 2008. Mapping surface roughness and soil moisture using multi-angle radar imagery without ancillary data. *Remote Sens. Environ.* 112, 391–402.
- Rosenqvist, A., Shimada, M., Suzuki, S., Ohgushi, F., Tadono, T., Watanabe, M., Tsuzuku, K., Watanabe, T., Kamijo, S., Aoki, E., 2014. Operational performance of the ALOS global systematic acquisition strategy and observation plans for ALOS-2 PALSAR-2. *Remote Sens. Environ.* 155, 3–12.
- Satalino, G., Mattia, F., Davidson, M.W., Le Toan, T., Pasquariello, G., Borgeaud, M., 2002. On current limits of soil moisture retrieval from ERS-SAR data. *IEEE Trans. Geosci. Remote Sens.* 40, 2438–2447.
- Satalino, G., Panciera, R., Balenzano, A., Mattia, F., Walker, J., 2012. COSMO-SkyMed multi-temporal data for land cover classification and soil moisture retrieval over an agricultural site in southern Australia. In: *Geoscience and Remote Sensing Symposium (IGARSS)*, 2012 IEEE International. IEEE, pp. 5701–5704.
- Shen, X., Mao, K., Qin, Q., Hong, Y., Zhang, G., 2013. Bare surface soil moisture estimation using double-angle and dual-polarization L-band radar data. *IEEE Trans. Geosci. Remote Sens.* 51, 3931–3942.
- Shimada, M., Isoguchi, O., Tadono, T., Isono, K., 2009. PALSAR radiometric and geometric calibration. *IEEE Trans. Geosci. Remote Sens.* 47, 3915–3932.
- Taylor, K.E., 2001. Summarizing multiple aspects of model performance in a single diagram. *J. Geophys. Res.-Atmos.* 106, 7183–7192.
- Thoma, D., Moran, M., Bryant, R., Rahman, M., Holifield-Collins, C., Skirvin, S., Sano, E., Slocum, K., 2006. Comparison of four models to determine surface soil moisture from C-band radar imagery in a sparsely vegetated semiarid landscape. *Water Resour. Res.* 42.
- Tsang, L., Kong, J.A., Shin, R.T., 1985. *Theory of Microwave Remote Sensing*. Wiley, New York.
- Ulaby, F.T., Bare, J., 1979. Look direction modulation function of the radar backscattering coefficient of agricultural fields. *Photogramm. Eng. Remote. Sens.* 45 (11), 1495–1506.
- Ulaby, F.T., Sarabandi, K., McDonald, K., Whitt, M., Dobson, M.C., 1990. Michigan microwave canopy scattering model. *Int. J. Remote Sens.* 11, 1223–1253.
- Ulaby, F.T., Long, D.G., Blackwell, W.J., Elachi, C., Fung, A.K., Ruf, C., Sarabandi, K., Zebker, H.A., Van Zyl, J., 2014. *Microwave Radar and Radiometric Remote Sensing*. The University of Michigan Press, Ann Arbor.
- van der Velde, R., Su, Z., van Oevelen, P., Wen, J., Ma, Y., Salama, M.S., 2012. Soil moisture mapping over the central part of the Tibetan Plateau using a series of ASAR WS images. *Remote Sens. Environ.* 120, 175–187.
- Wagner, W., Noll, J., Borgeaud, M., Rott, H., 1999. Monitoring soil moisture over the Canadian prairies with the ERS scatterometer. *IEEE Trans. Geosci. Remote Sens.* 37, 206–216.
- Walker, J.P., Houser, P.R., 2004. Requirements of a global near-surface soil moisture satellite mission: accuracy, repeat time, and spatial resolution. *Adv. Water Resour.* 27, 785–801.
- Wegmüller, U., Santoro, M., Mattia, F., Balenzano, A., Satalino, G., Marzahn, P., Fischer, G., Ludwig, R., Floury, N., 2011. Progress in the understanding of narrow directional microwave scattering of agricultural fields. *Remote Sens. Environ.* 115, 2423–2433.
- Wickel, A., Jackson, T., Wood, E., 2001. Multitemporal monitoring of soil moisture with RADARSAT SAR during the 1997 southern Great Plains hydrology experiment. *Int. J. Remote Sens.* 22, 1571–1583.
- Ye, N., Walker, J.P., Wu, X., Jackson, T., Renzullo, L., Merlin, O., Rüdiger, C., Entekhabi, D., DeJeu, R., Kim, E., 2016. Towards validation of SMAP: SMAPEX-4 & 5. In: 2016 IEEE International Geoscience and Remote Sensing Symposium (IGARSS), pp. 3469–3472.
- Zhang, X., Chen, B., Fan, H., Huang, J., Zhao, H., 2016. The potential use of multi-band SAR data for soil moisture retrieval over bare agricultural areas: Hebei, China. *Remote Sens.* 8, 7.
- Zhu, L., Walker, J.P., Ye, N., Rüdiger, C., 2016. The effect of radar configuration on effective correlation length. In: *Electromagnetics in Advanced Applications (ICEAA)*, 2016 International Conference on. IEEE, pp. 820–823.
- Zhu, L., Walker, J.P., Ye, N., Rüdiger, C., Hacker, J., Panciera, R., Tanase, M.A., Wu, X., Gray, D., Stacy, N., Goh, A., Yardley, H., Mead, J., 2018. The polarimetric L-band imaging synthetic aperture radar (PLIS): description, calibration and cross-validation. *IEEE J. Sel. Top. Appl. Earth Observ. Remote Sens.* 11, 4513–4525.
- Zhu, L., Walker, J.P., Ye, N., Rüdiger, C., 2019. Roughness and vegetation change detection: a pre-processing for soil moisture retrieval from multi-temporal SAR imagery. *Remote Sens. Environ.* 225, 93–106.
- Zribi, M., Dechambre, M., 2003. A new empirical model to retrieve soil moisture and roughness from C-band radar data. *Remote Sens. Environ.* 84, 42–52.
- Zribi, M., Taconet, O., Giarletti, V., Vidal-Madjar, D., 2002. Effect of row structures on radar microwave measurements over soil surface. *Int. J. Remote Sens.* 23, 5211–5224.
- Zribi, M., Baghdadi, N., Holah, N., Fafin, O., 2005. New methodology for soil surface moisture estimation and its application to ENVISAT-ASAR multi-incidence data inversion. *Remote Sens. Environ.* 96, 485–496.